Journal of
Applied
Crystallography

ISSN 1600-5767

Received 6 November 2014
Accepted 29 December 2014

Structure and stacking order in crystals of asymmetric dumbbell-like colloids

Antara Pal, Janne-Mieke Meijer, Joost R. Wolters, Willem K. Kegel and Andrei V. Petukhov*

Van 't Hoff Laboratory for Physical and Colloid Chemistry, Debye Institute for NanoMaterials Science, Utrecht University, Padualaan 8, 3584 CH, Utrecht, The Netherlands. Correspondence e-mail: a.v.petukhov@uu.nl

The crystalline structure assembled out of charge-stabilized asymmetric dumbbell-like colloidal particles in ethyl alcohol by sedimentation has been probed using small-angle X-ray scattering with microradian resolution. The existence of plastic face-centered cubic crystals was inferred from the observed Bragg peaks. The presence of stacking faults and the mosaic structure of the sample lead to the appearance of diffuse scattering, forming Bragg scattering cylinders in the three-dimensional reciprocal space. The quality of the crystalline structure, as ascertained from a detailed analysis of the diffuse scattering intensity distribution, indicates the presence of only 1.5% of stacking faults between the hexagonal close-packed layers.

1. Introduction

Ubiquitous thermal vibration of atoms gives rise to diffuse scattering (DS) in ideal crystals. In real crystals, however, the major contribution towards DS results from the various imperfections in the crystalline structures (Guinier, 1994; Wilson & Wilson, 1962). The nature of defects as well as their spatial distribution plays quite a significant role in influencing not only processes like critical fluctuation, nucleation and percolation but also numerous properties of a crystal, for example mechanical, magnetic, electronic and optical properties to name but a few. In contrast to Bragg diffraction, which only carries information regarding the average crystal structure, one can extract much more information from the diffuse intensity distribution in three-dimensional reciprocal space. The diffuse intensity distribution documents the correlated disorder that characterizes various defects present in a crystal structure. Therefore, an exhaustive analysis of DS in principle can act as a powerful tool towards identifying and analyzing various structural and compositional inhomogeneities in a crystalline structure. Depending on the nature of the disorder, various types of DS features are manifested in three-dimensional Fourier space in the form of DS planes and rods (Glazer *et al.*, 2004; Baba-Kishi *et al.*, 2008; Welberry *et al.*, 2010; Burkovsky *et al.*, 2012), lenses (Bosak *et al.*, 2009), butterflies (Bosak *et al.*, 2012) *etc*.

Large-scale structures, such as colloidal and photonic crystals, usually contain a significant amount of disorder which strongly influences their functional properties. Therefore, it is important to characterize in detail not only the crystal structure but also the defects present. In addition, colloidal crystals show stacking disorder that is interesting from a fundamental point of view with respect to the formation of close-packed structures.

Colloidal hard spheres are known to self-organize into close-packed structures that consist of stacks of hexagonal close-packed planes. Periodic stacking of these planes in *ABCABC* or *ABABAB* sequences leads to the formation of face-centered cubic (f.c.c.) or hexagonal close-packed (h.c.p.) structures, respectively. Since the free energy difference between these two structures is quite small, $\sim 10^{-3} k_{\rm B}T$ per particle in favor of the f.c.c. structure (where $k_{\rm B}$ is the Boltzmann constant and T the temperature) (Bolhuis *et al.*, 1997; Bruce *et al.*, 1997; Mau & Huse, 1999), spheres are often found to be stacked in a random mixture of these two particular stacking types (Dolbnya *et al.*, 2005; Zhu *et al.*, 1997; Kegel & Dhont, 2000), resulting in the formation of a random hexagonal close-packed (r.h.c.p.) structure. Stacking disorder of these types has been studied in great detail using several scattering techniques such as light scattering and small-angle X-ray and neutron scattering (Wilson, 1942; Dux & Versmold, 1997; Versmold, 1995; Petukhov *et al.*, 2003; Byelov *et al.*, 2010; Meijer *et al.*, 2014; Vos *et al.*, 1997). The stacking disorder in scattering experiments manifests itself as the smearing out of some of the Bragg reflections along the so-called Bragg scattering rods in the direction perpendicular to the planar stacking faults.

In this article, we report an X-ray scattering study of self-assembled crystals of asymmetric dumbbell-like colloids. Charge-stabilized asymmetric dumbbell-like colloidal particles in ethyl alcohol have been crystallized by gravity-induced osmotic pressure. Investigation by microradian X-ray scattering reveals the crystal structure to be an f.c.c. plastic crystal containing only 1.5% of stacking faults. Our data further

reveal a new DS feature in three-dimensional reciprocal space in the form of Bragg scattering cylinders.

2. Synthesis and characterization

2.1. Synthesis

The dumbbell particles studied here were synthesized using seeded emulsion polymerization as described in detail by Mock *et al.* (2006). First, monodisperse cross-linked polystyrene spheres (CPSs) were prepared using emulsion polymerization. The cross-linking density was ∼3%. The CPS particles were subsequently coated with vinyl acetate (surface coverage 21.36×10^{-21} g nm^{-2}) in order to increase the hydrophilicity of the surface. The particles were then swelled with a desired amount of styrene. For the present case the swelling ratio S, which is defined as $S = W_m/W_p$, W_m and W_p being the weight of the swelling monomer and of the seed polymer, respectively, was fixed at a value 5. The samples were stirred vigorously during swelling for about two days and subsequently placed in a 353 K oil bath. The heating causes phase separation of the monomer taken up by the cross-linked polymer network, resulting in the formation of a droplet on the colloidal surface. The hydrophilicity of the surface determines the wetting angle between the monomer and the colloidal surface. Subsequent polymerization was carried out at 535 K by addition of azobisisobutyronitrile (0.94 mg AIBN dissolved in 0.046 ml of styrene per millilitre of seed suspension) and hydroquinone (0.75 m*M*, 99% purity, Riedel), a water soluble inhibitor. Polymerization was allowed to continue for 24 h. Finally, the particles were washed with deionized water and the solvent was then replaced by ethyl alcohol by several centrifugation and redispersion cycles.

2.2. Characterization and methods

The size of the dumbbell-like colloidal particles was characterized using transmission electron microscopy (TEM) (Philips TECNAI 10) (Forster *et al.*, 2011; Hosein *et al.*, 2010). Figs. 1(*a*) and 1(*b*) show the TEM image and the particle size distribution. The particle length l, seed particle radius r_s and protrusion radius r_p were found to be l = 323 nm, r_s = 112 nm and r_p = 139 nm.

Small-angle X-ray scattering experiments were performed at the Dutch–Belgian beamline BM-26B of the European Synchrotron Radiation Facility (ESRF) in Grenoble, France (Borsboom *et al.*, 1998), using a microradian diffraction setup (Petukhov *et al.*, 2006; Thijssen *et al.*, 2006). A compound refractive lens was used just after the sample in order to focus the transmitted and diffracted beams at the detector screen, thus increasing the q-space resolution. The wavelength of the X-rays used was λ = 0.9537 Å. The diffraction patterns were recorded using a Pilatus 1M detector of pixel size 172 × 172 µm with angular resolution ∼11 µrad. Since the resolution of the Pilatus detector was limited by its pixel size, for higher-resolution data a 16 bit CCD camera (Photonic Science, Xios II) with a pixel size of 9 × 9 µm was used, for which the angular resolution was ∼5 µrad. To explore the colloidal superstructures formed, several rectangular capillaries (100 × 3 × 0.2 mm) were filled with a suspension of colloidal particles (∼50 µl) and kept for at least six months for sedimentation. All the capillaries were visually inspected after six months under white-light illumination. The iridescent colors caused by Bragg reflections were the first indication of the presence of ordered structures in them. Fig. 1(*c*) shows a photograph of such a capillary, indicating the presence of a crystal within it. During X-ray diffraction measurement, these capillaries were attached to a goniometer that can rotate the capillary around

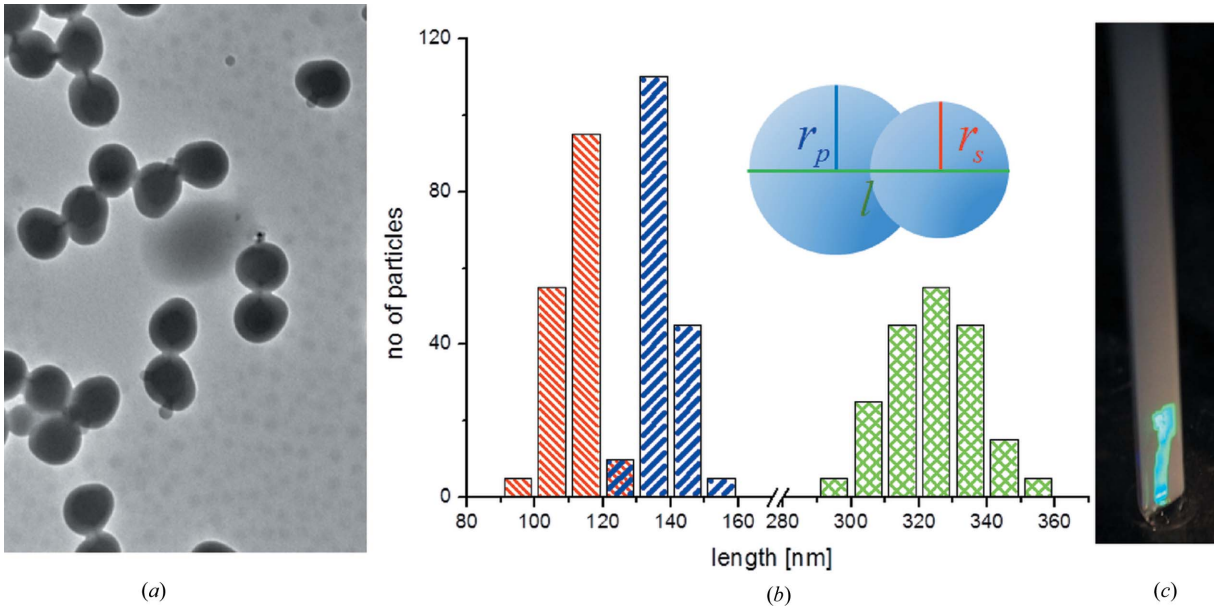

Figure 1
(*a*) TEM image of asymmetric dumbbells and (*b*) their size distribution. The red, blue and green data indicate the seed particle radius r_s, the protrusion radius r_p and the length of the particles l, respectively. (*c*) Capillary showing the Bragg reflection that indicates the presence of a crystal.

its vertical axis. As a result of this rotation, the angle between the incident X-ray beam and the structure formed inside the capillary can be changed, giving an opportunity to explore the full three-dimensional reciprocal space. For normal incidence the direction of the X-ray beam was perpendicular to the surface of the capillary. We define this position as $\omega = 0^\circ$, ω being the angle between the X-ray beam and the normal to the surface of the capillary, which was varied between -70 and $+70^\circ$ in steps of 0.1°.

3. Results

The sharp diffraction features observed in the diffraction pattern in Fig. 2 (inset), taken at a height of $h = 5.5$ mm from the bottom of the capillary, indicate the presence of a set of highly ordered colloidal crystals within the irradiated area. These features are found along concentric rings and are clearly visible in the radial intensity profile shown by the dashed line in Fig. 2. The vertical lines indicate the q values related as $1{:}3^{1/2}{:}4^{1/2}{:}7^{1/2}{:}9^{1/2}$, which is a characteristic feature of hexagonal packing. Peaks at four of these q values can be observed in the profile. The absence of the $4^{1/2}$ peak can be attributed to its superposition with the form factor minimum, shown by the red line in Fig. 2. The circular nature of the diffraction pattern indicates the presence of multiple domains in the crystal.

In order to determine the three-dimensional crystal structure, the capillary was rotated about its vertical axis by a rotation angle ω as shown in Fig. 3. At $\omega = 15^\circ$, the first-order ring is still clearly visible, while the $3^{1/2}$ ring disappears, indicating that the first ring corresponds to an extended feature while the other ring arises from a localized feature. (x', y', z') represents the laboratory frame of reference. At $\omega = 0^\circ$, the laboratory frame is superimposed with the crystallographic frame of reference (X, Y, Z). Since the capillary is rotated about its vertical axis, which is y', at all other angles y' and the Y axis are equivalent.

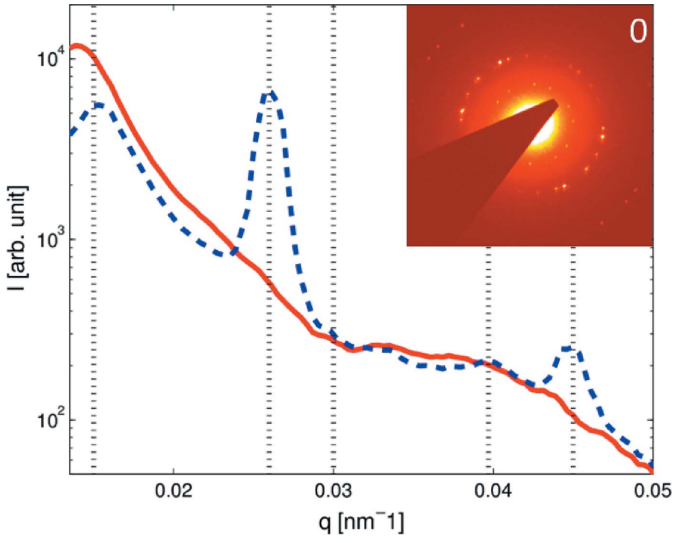

Figure 2
Radially averaged intensity profiles as a function of scattering vector magnitude q, representing the crystal (blue dashed line) and the form factor (red solid line). The form factor is measured at a height in the capillary that is much above the sediment and the corresponding intensity is rescaled for better visualization. Inset: diffraction pattern taken at a height of $h = 5.5$ mm from the bottom of the capillary.

Further, with the rotation of the capillary, the diffraction spots of which the first-order ring is composed gradually start to move in the direction of increasing $|q_x|$. As a result, the diffraction pattern gets stretched in the horizontal direction and the first-order ring eventually changes its shape from a circle to an ellipse, which is very clear at $\omega = 35^\circ$ (Fig. 3). The ellipticity is further enhanced at 45 and 55°. This monotonic change of the scattering vector $\mathbf{q}$ as a function of ω is quite unusual. Usually, a Bragg reflection arising from a crystal has a well defined value of $\mathbf{q}$. With rotation of the crystal one expects the reflection to vanish since the Bragg condition will not be satisfied anymore. This special behavior of the diffraction peaks can be explained by the presence of extended one-dimensional features (shown in Fig. S1[1]) in the reciprocal space, which are elongated along the crystallographic Z axis or normal to the capillary surface, as a change in ω enables one to explore the intensity along the crystallographic Z-axis direction. As shown in detail in the supporting information, these elongated features are straight lines that can be attributed to the presence of two-dimensional planar defects such as stacking faults parallel to the capillary wall.

In addition to the elongated features, there are some very strong diffraction peaks which appear at certain angles (ω). The width of these peaks as a function of ω is very narrow. The sharpness of these peaks indicates that they are Bragg spots and are localized at a particular point in the three-dimensional Fourier space.

The generic reciprocal lattice of a close-packed crystal is schematically depicted in Fig. 4. The diffraction is observed at wavevectors $\mathbf{q} = h\mathbf{b}_1 + k\mathbf{b}_2 + l\mathbf{b}_3$, where h and k must be integers because of the in-plane periodicity. For $(h - k)$ divisible by 3 the reflection does not depend on the stacking order and is only observed at integer values of l. For $(h - k)$ not divisible by 3 the diffraction intensity sensitively depends on the stacking order. For an r.h.c.p. structure, with a random mixture of f.c.c. and h.c.p. stacking types, one observes so-called Bragg scattering rods (Dolbnya *et al.*, 2005; Petukhov *et al.*, 2003, 2002) with monotonically varying structure factor $S(q)$ along them. However, if the f.c.c. structure dominates then sharp $S(q)$ peaks appear at $l = 1/3 + n$ or $l = 2/3 + n$ depending on the type of Bragg rod and the stacking direction (*ABCABC* or *ACBACB*). Hence the appearance of the strong localized stacking-independent peak around $\omega = 25^\circ$ (see Fig. 3) confirms the overall crystal structure to be close-packed f.c.c.

The two-dimensional texture of the diffraction pattern at $\omega = 0^\circ$ (Fig. 3) indicates that the crystal consists of many domains. Its circular nature proves that the hexagonal planes in these domains are parallel to the flat substrate, while their azimuthal orientations are different. Since all the hexagonal

[1] Supporting information for this paper is available from the IUCr electronic archives (Reference: VH5024).

planes are parallel to the glass substrate, we can conclude that the crystal growth is heterogeneously nucleated at the capillary walls and slowly progresses towards the center of the capillary. In the case where there are multiple crystals present in a sample, which all consist of hexagonal close-packed planes parallel to the capillary wall while their lateral orientation is randomized, the reciprocal lattice can be obtained from the single-crystal lattice by performing azimuthal smearing around the axis normal to the substrate surface (vertical axis in Fig. 4). For such a two-dimensional texture the sharp stacking-independent Bragg reflections can then be found along circles, while the Bragg rods end up on the surface of cylinders called Bragg cylinders, as illustrated in Fig. 4. At $\omega = 0^\circ$, the intersection of the (10l) Bragg cylinder and Ewald sphere appears as a circle (Fig. S2). This circle is visible in the diffraction pattern corresponding to $\omega = 0^\circ$ in Fig. 3. As the capillary is rotated about the y' axis, this intersection becomes elliptical as observed for the consecutive angles (Figs. S2 and 3). This experimental fact leads us to believe that there are stacking faults present in our crystal, leading to the formation of the DS feature, *i.e.* the Bragg cylinder, in the diffraction pattern. The observation of the Bragg cylinder is remarkable as such features have never been shown for colloidal crystals before.

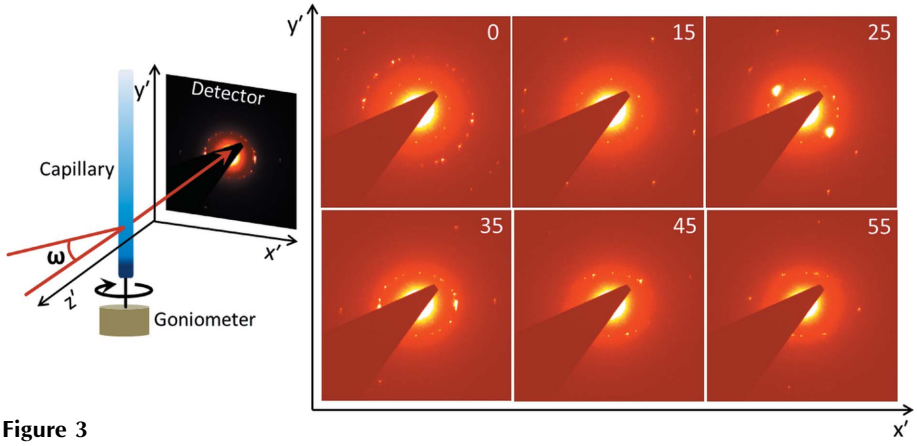

Figure 3
The left panel shows the rotation scheme of the capillary, while the right one represents the diffraction patterns of the crystal at different rotation angles ω. (x', y', z') represents the laboratory frame of reference. At $\omega = 0^\circ$ the laboratory frame is superimposed with the crystallographic frame of reference (X, Y, Z). Since the capillary is rotated about its vertical axis, which is y', at all other angles y' and the Y axis are equivalent.

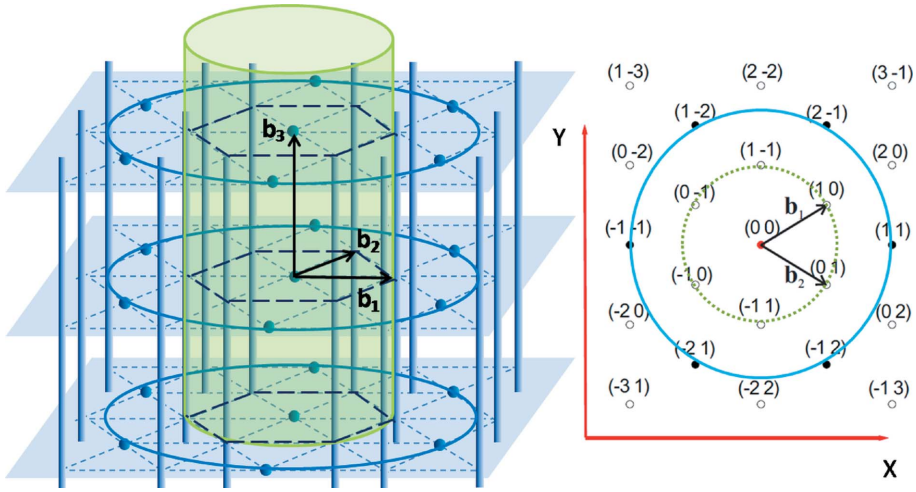

Figure 4
Reciprocal lattice of close-packed two-dimensional texture with stacking faults. The left panel shows the side view, while the right one shows the top view of the lattice. Because of the azimuthal smearing, each Bragg peak lies on a circle, while each Bragg rod lies on the surface of a Bragg cylinder. Examples of those circles and cylinders are shown by blue and green objects, respectively.

As already mentioned, the effect of stacking faults is reflected as the intensity modulation along the Bragg rods forming the cylinders. By rotating the crystal about the y' axis, one can explore this modulation (Fig. S1) and hence quantify the stacking order. From the intensity distribution along the first- and second-order Bragg rods, one can also learn about the structure of the crystal under investigation. This intensity distribution is usually described by either Wilson's theory (Wilson, 1942) or a modification of Wilson's theory (Paterson, 1952; Hilhorst *et al.*, 2009). Wilson's original theory is valid if a single h.c.p. layer changes the direction of the f.c.c. growth from the ABC to ACB type stacking. Both the growth directions (positive and negative **x** direction) are then equally present. The modified model is applicable when only one growth direction dominates. This can only happen if the stacking disorder is caused by pairs of h.c.p. layers. Such 'double' stacking faults are in fact a small fraction of layers stacked the other way, creating the stacking faults. The variation of the structure factor along the (hk) Bragg rod $S_{hk}(l)$ is a result of interference of the contributions of different layers and can be represented as [see the supplementary information of Hilhorst *et al.* (2009)]

$$S_{hk}(l) = \mathrm{Re}\Big[\big(1 + \exp\{2\pi i[l - (h-k)/3]\} \times \{1 - \beta + \beta\exp[4\pi i(h-k)/3]\}\big) / \big(1 - \exp\{2\pi i[l - (h-k)/3]\} \times \{1 - \beta + \beta\exp[4\pi i(h-k)/3]\}\big)\Big]. \quad (1)$$

The diffracted intensity $I(q)$ is proportional to the product of the form factor $P(q)$, the scattering by a single particle, and the structure factor $S(q)$, arising from the interparticle positional correlations, and can be represented as

$$I(q) = A\,P(q)\,S(q), \quad (2)$$

A being the scaling factor depending on the experimental details.

In Fig. 5, the blue dots represent the experimentally obtained variation of intensity as a function of l. The conversion from ω to l is discussed in the supporting information. The top panel shows the (10l) Bragg rod, while the bottom panel indicates the (20l) Bragg rod. The red lines indicate the fit by using equations (1) and (2) with a fitting parameter β which is found to be 0.015. For $P(q)$ we have used the experimentally measured form factor, shown by the red continuous line in Fig. 2. The value of β suggests that only 1.5% of the layers are stacked in the opposite direction from that of the remaining 98.5% of layers, resulting in a very good quality f.c.c. crystal. This is a very high degree of stacking order for colloidal crystals, which are prone to stack in a disordered manner. Moreover, since the (10l) Bragg rod shows a strong peak around $l = 1/3$, we can say that the stacking of hexagonal layers has a predominant $ABCABC$ stacking sequence, as already discussed in the previous section.

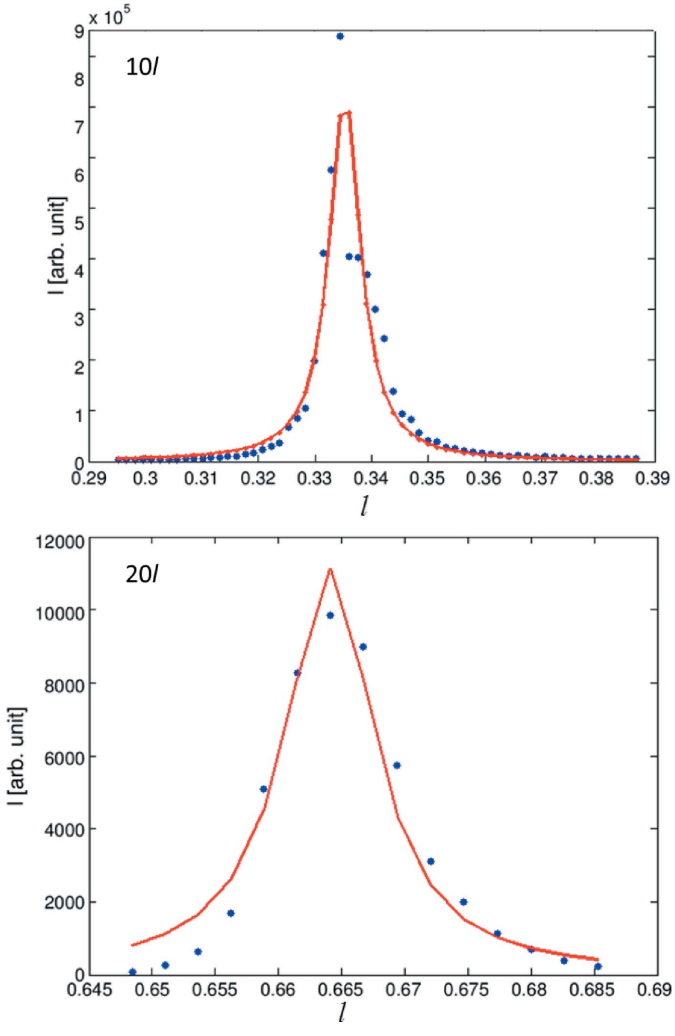

Figure 5
Variation of intensity I as a function of l for (10l) and (20l) Bragg rods. The blue dots represent the experimental data, while the red lines indicate the best fit using equations (1) and (2).

4. Discussion and conclusion

Using microradian X-ray scattering, we have probed in detail the f.c.c. plastic crystal structure formed by anisotropic dumbbell-like colloidal particles. In colloidal systems, when the sedimentation rate is quite low, particles have enough time to find their equilibrium positions before the layer structure gets arrested by further crystal growth (Pusey *et al.*, 1989; Hoogenboom *et al.*, 2002). In addition, the presence of a soft repulsive interaction (*e.g.* electrostatic interaction in the case of charged colloids) between these particles further lowers the energy barrier for the rearrangement of layers in favor of the thermodynamically stable f.c.c. structure, resulting in crystalline structures having dominant f.c.c. stacking order rather than h.c.p. (Vos *et al.*, 1997).

Since the particles used in this study are charge stabilized, the interparticle interaction energy is determined by a balance between the double layer repulsion and the van der Waals attraction. The range of this repulsive interaction is determined by the Debye screening length, κ^{-1}, which in turn is related to the dielectric constant, ε_r, and ionic strength, I, of the solvent by the relation $\kappa^{-1} = (\varepsilon_0\,\varepsilon_r\,k_B T/2\,N_A e^2\,I)^{1/2}$, where ε_0 is the permittivity of free space, N_A is Avogadro's number and e is the charge of an electron. For pure ethanol, $\varepsilon_r = 20$ and ionic concentration $\sim 10^{-5}\,M$, κ^{-1} can reach up to 48 nm. Consequently, the effective shape of the particles appears to be spherical and their anisotropy does not show up in the diffraction pattern for normal incidence, which is clear from Fig. 2 (inset). This experimental observation leads us to believe that the resulting f.c.c. crystal is plastic in nature. The largest dimension of the particles as obtained from the TEM measurement is the length of the particles, which is 323 nm. However, the d spacing corresponding to the first-order peak is found to be 409 nm, which would correspond to a particle diameter of 472 nm. The large value of the Debye length is responsible for this high value of the observed d spacing. Further, the large value of the Debye length also explains the small number of stacking faults in the crystalline structure. Moreover, the smaller buoyant mass of these particles plays an important role in slowing down their sedimentation rate, which promotes the formation of a crystalline structure with a lower number of stacking faults.

The most important outcome of this study is the visualization of Bragg cylinders. As a consequence of the heterogeneous nucleation, which starts from the substrate, all the hexagonal layers of the different crystallites have one axis fixed and their azimuthal orientation randomized. This provides the right conditions for the formation of the particular DS feature called the Bragg cylinder, which can be directly visualized from the diffraction patterns and used to quantify the degree of stacking faults.

AP thanks the Netherlands Organization for Scientific Research (NWO) (700.10.355). The personnel of the DUBBLE beamline are thanked for their help with the synchrotron experiment, and NWO is thanked for granting beam time.

References

Baba-Kishi, K. Z., Welberry, T. R. & Withers, R. L. (2008). *J. Appl. Cryst.* **41**, 930–938.

Bolhuis, P. G., Frenkel, D., Mau, S.-C. & Huse, D. A. (1997). *Nature*, **388**, 235–236.

Borsboom, M., Bras, W., Cerjak, I., Detollenaere, D., Glastra van Loon, D., Goedtkindt, P., Konijnenburg, M., Lassing, P., Levine, Y. K., Munneke, B., Oversluizen, M., van Tol, R. & Vlieg, E. (1998). *J. Synchrotron Rad.* **5**, 518–520.

Bosak, A., Chernyshov, D., Vakhrushev, S. & Krisch, M. (2012). *Acta Cryst.* A**68**, 117–123.

Bosak, A., Hoesch, M., Krisch, M., Chernyshov, D., Pattison, P., Schulze-Briese, C., Winkler, B., Milman, V., Refson, K., Antonangeli, D. & Farber, D. (2009). *Phys. Rev. Lett.* **103**, 076403.

Bruce, A., Wilding, N. & Ackland, G. (1997). *Phys. Rev. Lett.* **79**, 3002–3005.

Burkovsky, R., Bronwald, Y. A., Filimonov, A., Rudskoy, A., Chernyshov, D., Bosak, A., Hlinka, J., Long, X., Ye, Z.-G. & Vakhrushev, S. (2012). *Phys. Rev. Lett.* **109**, 097603.

Byelov, D. V., Hilhorst, J., Leferink op Reinink, A. B., Snigireva, I., Snigirev, A., Vaughan, G. B., Portale, G. & Petukhov, A. V. (2010). *Phase Transitions*, **83**, 107–114.

Dolbnya, I., Petukhov, A., Aarts, D., Vroege, G. & Lekkerkerker, H. (2005). *Europhys. Lett.* **72**, 962–968.

Dux, C. & Versmold, H. (1997). *Phys. Rev. Lett.* **78**, 1811–1814.

Forster, J. D., Park, J.-G., Mittal, M., Noh, H., Schreck, C. F., O'Hern, C. S., Cao, H., Furst, E. M. & Dufresne, E. R. (2011). *ACS Nano*, **5**, 6695–6700.

Glazer, A., Thomas, P., Baba-Kishi, K., Pang, G. & Tai, C. (2004). *Phys. Rev. B*, **70**, 184123.

Guinier, A. (1994). *X-ray Diffraction in Crystals, Imperfect Crystals, and Amorphous Bodies.* Mineola: Dover Publications.

Hilhorst, J., Abramova, V. V., Sinitskii, A., Sapoletova, N. A., Napolskii, K. S., Eliseev, A. A., Byelov, D. V., Grigoryeva, N. A., Vasilieva, A. V., Bouwman, W. G., Kvashnina, K., Snigirev, A., Grigoriev, S. V. & Petukhov, A. V. (2009). *Langmuir*, **25**, 10408–10412.

Hoogenboom, J. P., Derks, D., Vergeer, P. & van Blaaderen, A. (2002). *J. Chem. Phys.* **117**, 11320–11328.

Hosein, I. D., Lee, S. H. & Liddell, C. M. (2010). *Adv. Funct. Mater.* **20**, 3085–3091.

Kegel, W. K. & Dhont, J. K. (2000). *J. Chem. Phys.* **112**, 3431–3436.

Mau, S.-C. & Huse, D. A. (1999). *Phys. Rev. E*, **59**, 4396–4401.

Meijer, J. M., Shabalin, A., Dronyak, R., Yefanov, O. M., Singer, A., Kurta, R. P., Lorenz, U., Gorobstov, O., Dzhigaev, D., Gulden, J., Byelov, D. V., Zozulya, A. V., Sprung, M., Vartanyants, I. A. & Petukhov, A. V. (2014). *J. Appl. Cryst.* **47**, 1199–1204.

Mock, E. B., De Bruyn, H., Hawkett, B. S., Gilbert, R. G. & Zukoski, C. F. (2006). *Langmuir*, **22**, 4037–4043.

Paterson, M. S. (1952). *J. Appl. Phys.* **23**, 805–811.

Petukhov, A., Aarts, D., Dolbnya, I., De Hoog, E., Kassapidou, K., Vroege, G., Bras, W. & Lekkerkerker, H. (2002). *Phys. Rev. Lett.* **88**, 208301.

Petukhov, A., Dolbnya, I., Aarts, D., Vroege, G. & Lekkerkerker, H. (2003). *Phys. Rev. Lett.* **90**, 028304.

Petukhov, A. V., Thijssen, J. H. J., 't Hart, D. C., Imhof, A., van Blaaderen, A., Dolbnya, I. P., Snigirev, A., Moussaïd, A. S. I. & Snigireva, I. (2006). *J. Appl. Cryst.* **39**, 137–144.

Pusey, P. N., van Megen, W., Bartlett, P., Ackerson, B. J., Rarity, J. G. & Underwood, S. M. (1989). *Phys. Rev. Lett.* **63**, 2753–2756.

Thijssen, J. H., Petukhov, A. V., 't Hart, D. C., Imhof, A., van der Werf, C. H., Schropp, R. E. & van Blaaderen, A. (2006). *Adv. Mater.* **18**, 1662–1666.

Versmold, H. (1995). *Phys. Rev. Lett.* **75**, 763–766.

Vos, W. L., Megens, M., van Kats, C. M. & Bösecke, P. (1997). *Langmuir*, **13**, 6004–6008.

Welberry, T., Goossens, D., Withers, R. & Baba-Kishi, K. (2010). *Metall. Mater. Trans. A*, **41**, 1110–1118.

Wilson, A. C. (1942). *Proc. R. Soc. London Ser. A*, **180**, 277–285.

Wilson, A. J. C. & Wilson, A. (1962). *X-ray Optics: the Diffraction of X-rays by Finite and Imperfect Crystals.* London: Methuen.

Zhu, J., Li, M., Rogers, R., Meyer, W., Ottewill, R. H., STS-73 Space Shuttle Crew, Russel, W. B. & Chaikin, P. M. (1997). *Nature*, **387**, 883–885.